Analyse du transport de chaleur et de masse dans un milieu poreux complexe à base de PDMS.

Analysis of heat and mass transport in a complex PDMS-based porous medium.

Emil Grigorov[1*], **Yann Jobic**[1], **Frederic Topin**[1]

[1]Aix Marseille Université, CNRS, IUSTI UMR 7343, 13453, Marseille, France

Résumé - Dans cette étude, nous déterminons numériquement certaines propriétés géométriques, comme la conductivité thermique effective, le tenseur de perméabilité et la composante longitudinale du tenseur de dispersion pour l'écoulement d'un fluide dans un milieu poreux de polydiméthylsiloxane (PDMS). Un modèle tridimensionnel est reconstruit à l'aide d'images de microtomographie, en suivant la méthodologie décrite dans [6]. L'objectif de cet article est présenter la méthodologie et les premiers résultat pour l'analyse détaillée de la façon dont ces propriétés influencent le mélange des fluides, comme suggéré dans [6].

Abstract - In this study, we numerically determine geometrical properties, as effective thermal conductivity, permeability tensor, and the longitudinal component of the dispersion tensor for fluid flow within a porous polydimethylsiloxane (PDMS) medium. A three-dimensional model is reconstructed using microtomography images, following the methodology described in [6]. The objective of this paper is to introduce a methodology along with first results for the detailed analysis of how these properties influence fluid mixing, as suggested in [6]. The results of this analysis will be presented in a future publication.

Nomenclature

M	mixing efficiency, $\%$	T	temperature, K
D	mass diffusivity, m^2/s	*Greek symbols*	
D^*	dispersion tensor	τ	tortuosity
L	length, m	$\boldsymbol{\phi}$	heat flux, W/m^2
K	permeability, m^2	λ	heat conductivity, W/mK
P	pressure, Pa	μ	dynamic viscosity, $\mathrm{Pa\ s}$
$\mathbf{V}$	velocity vector	∇	gradient operator
$\tilde{\mathbf{v}}$	deviation of local velocity		
U	darcy velocity, m/s	*Index and exponent*	
$\mathbf{B}$	closure vector	f	fluid
$\mathbf{I}$	identity matrix	s	solid
N	number of control volumes	D	darcy
$\overline{c}$	average mass fraction		

1. Introduction

In many microfluidic applications, mixing is required to enable efficient reactions between two or more components. In this context, the low Reynolds numbers and the laminar flow in the microchannels mean that fluid mixing is heavily dependent on diffusion, which may cause the construction of channels with unacceptably long lengths. Based on oscillations in the flow field,

https://doi.org/10.25855/SFT2025-076

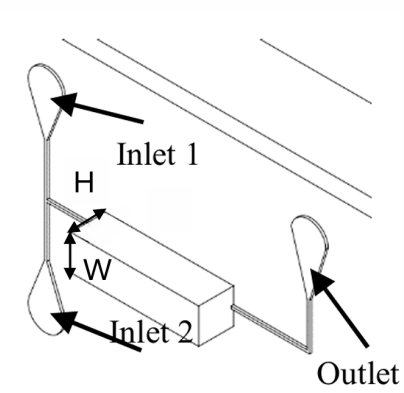

Figure 1 : *Schematic of the purposed device in [6] for the purposes of on-chip mixing*

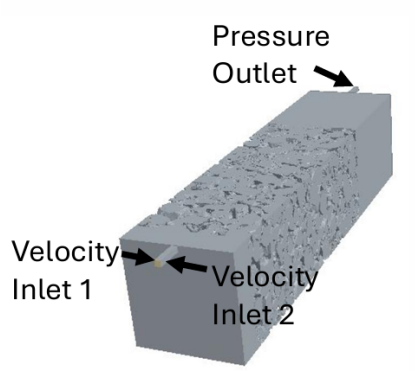

Figure 2 : *3D geometry of the numerical simulations, reconstructed from CT images*

active methods utilize external energy sources (e.g., acoustic waves [2]). However, the fabrication of these devices tends to be difficult because of the moving parts. Passive mixing, on the other hand, is achieved by changing the geometry of the channels during the fabrication stage, introducing various types of geometrical features, in order to accelerate the diffusion between the two fluids through fluid stretching and folding [1], [3]. All of the proposed geometries so far utilize the concept of ”chaotic advection” [4], where the fluid undergoes a series of unpredictable motions that disrupt fluid layers and enhance molecular exchange between different regions. Even though many novel passive mixers have been shown to efficiently achieve rapid mixing, they rely on relatively complex geometries with channels usually smaller than $10\,\mu\mathrm{m}$, requiring clean room facilities for their fabrication. Taking all of these considerations into account, it is known that chaotic advection occurs in porous media according to some studies [5]. Recently, in the work of Grigorov et al. [6], sugar cube was used as a template to create a random pore network made of polydimethylsiloxane (PDMS) polymer for the purpose of on-chip microfluidic mixing. The proposed geometry is easy to fabricate and the authors report promising efficiency in fluid mixing.

2. Numerical comparison with experimental data

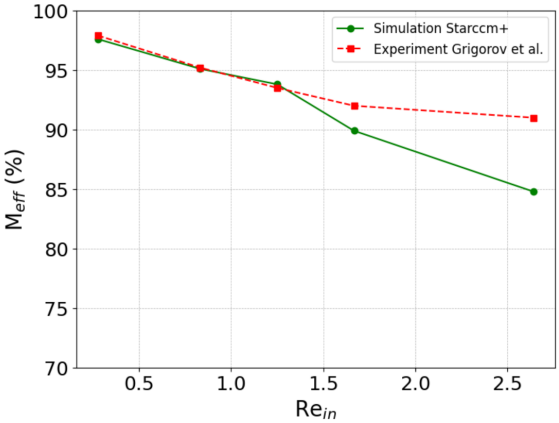

Figure 3 : *Comparison of the mixing index for experimental setup [6] and numerical simulation, which shows a good agreement.*

Based on CT images of the same structure described in [6], a 3D geometry of the sample is reconstructed to compare numerical simulations with the experimental results presented in [6], validating the mesh used for the further thermal and mass transport analyses and their impact on the mixing process. The fabrication process of the porous polymer medium is described in [6] and is as follows: The sugar cube infiltrated with a PDMS prepolymer mixture is subjected to a temperature of 60°C for 2 hours in an oven to ensure complete PDMS polymerization. Once the process is complete, the composite is transferred to a freezer for a duration of 3 minutes to facilitate detachment of the PDMS from the

polymer. Finally, the crystals are removed by rinsing with deionized water. The geometry of the device used in [6] is shown in Figure 1. The model consists of two inlet channels and one exit channel, each having dimensions of 200 x $200\,\mu\mathrm{m}$. For the validation of the numerical simulations presented here, the size of the mixing chamber was fixed at 4 x $4\,\mathrm{mm}$. The numerical simulations were performed with a polyhedral volume mesh (a mean size of about 0.2 mm with a total number of $15\,198\,255$ cells) that was generated for the fluid part using StarCCM+ mesher (Figure 2). .

A convection-diffusion equation is used to model the mixing problem. Similar to [6], self-diffusion of pure water is utilized for the simulations, with a diffusion coefficient of D = $2.29\,\mu\mathrm{m}^2\,\mathrm{ms}^{-1}$. Experiments were conducted using water and dye chosen to have similar properties. The mixing efficiency in the experiments of [6] was determined by analyzing the standard deviation of the average gray intensity of the pixels in a selected mixing region in the center of the channel, taken from microscopic images captured at the outlet of the mixing chamber. For the simulation in the current study, we use the same concept based on the average mass fraction on the exit plane after the mixing region:

$$M_{\text{eff}} = 1 - \sqrt{\frac{\frac{1}{N}\sum_{i=1}^{N}(\overline{c} - c_i)^2}{\overline{c}}}, \tag{1}$$

where c_i and $\overline{c}$ represent the mass fraction of the fluid in the i-th cell and the average mass fraction of the fluid over the entire cross-sectional area of the outflow, respectively.

Figure 3 shows the results from the cinducted comparison. The corresponding Reynolds (Re_{in}) number is based on the inlet velocity in [6]. For the first four points, the discrepancy is less than 3%. For the final point, the latter is approximately 5.3%, which is acceptable for the purposes of the current analysis.

In the next section, an analysis of the mass and thermal properties of the sample used in this study will be presented. For computational efficiency, one-quarter of the total domain length was utilized. The dimensions of the sample are about 5 pores in the X and Y directions and 4 along the Z. For this study we consider that the latter would constitute a reasonable representative elementary volume (REV).

3. Workflow for sample properties analysis

3.1. Geometry

The purpose of this paper is to introduce a workflow for the analysis of various thermal and mass transport properties of the porous medium under study. Figures 4 and 5 show the region of interest (ROI) for both fluid and solid phases utilized for the further analysis. The sample was scanned using X-ray computed tomography with a voxel size of $13\,\mu\mathrm{m}$. The selected ROI is centered to avoid edge effects caused by the walls and has a voxel size of 308 x 308 x 205. The geometrical analysis was performed using the open-source in-house software iMorph [7]. We estimated the phase volumetric fraction to be at 74.7% for the fluid and the 25.3% for the solid phase, with specific surface areas of $7553.8\,\mathrm{m}^2\,\mathrm{m}^{-3}$. The fluid plane-to-plane tortuosity, τ, was measured to be 1.019, 1.020, and 1.023 for the X, Y, and Z directions, respectively. For the analysis of the pore distribution, we used the software "iMorph". Figure 6 shows a three-dimensional representation of three typical pores, as well as a planar view of the segmented pores, represented by different colors. Clearly, the pore shape reproduces the crystalline nature

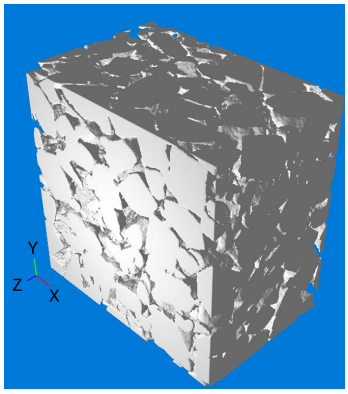

Figure 4 : *Region of interest chosen for the fluid phase*

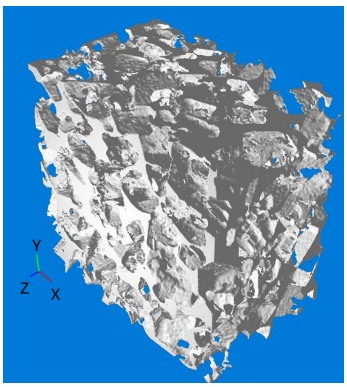

Figure 5 : *Region of interest chosen for the solid phase ; it is the complement of the fluid ROI*

of the sugar on which the PDMS was molded. To evaluate the size of a cell, we measured the radius r_p, which is defined as the equivalent sphere radius of a fluid volume equal to that of the cell. Figure 7 presents the cumulative volume distribution as a function of r_p. The median value of r_p, is found to be $225.6\,\mu\mathrm{m}$. More than three-fourths of the sample can be represented by spheres with a radius below $430\,\mu\mathrm{m}$, while only 10% consists of large pores. This indicates numerous constrictions in the poral space between the convex shapes.

4. Effective thermal conductivity

One of the key indicators of mass transport behavior in biological applications is the geometry's response to thermal stimulation, important for processes such as thermal cell lysis and DNA amplification. The temperature distribution influences consequently the dynamics of mixing and mass transport of reagents and samples. As a first step, we analyze the effective thermal conductivity of the sample. For the numerical modeling the methodology proposed in [8] was used, not taking into account radiative transfer, mass transfer at the interface or any

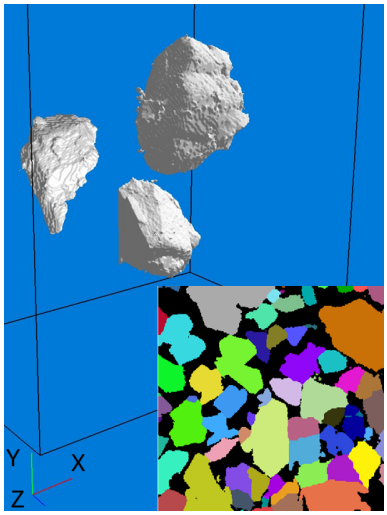

Figure 6 : *Three Dimensional representation of typical PDMS pores, together with a planar view on the pore distribution.*

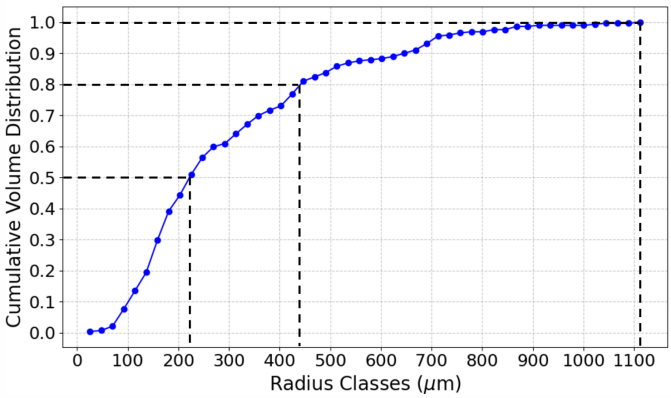

Figure 7 : *Volume distribution as a function of r_p*

chemical reaction. The equations of energy conservation are solved numerically over the entire volume of both fluid and solid phase (separately), which allows to obtain the temperature gradients and heat fluxes at any point of each of the phases. Using the well-known macroscopic two-temperature model [9] one can write for each phase (dropping subscript i for the considered phase):

$$\boldsymbol{\phi} = \overline{\overline{\lambda_{\text{eff}}}} \nabla \langle T \rangle, \ \overline{\overline{\lambda_{\text{eff}}}} = \begin{bmatrix} \lambda_{xx} & \lambda_{xy} & \lambda_{xz} \\ \lambda_{yx} & \lambda_{yy} & \lambda_{yz} \\ \lambda_{zx} & \lambda_{zy} & \lambda_{zz} \end{bmatrix}, \tag{2}$$

where $\boldsymbol{\phi}$ is the macroscopic phase heat flux, $\overline{\overline{\lambda_{\text{eff}}}}$ is the symmetric tensor of the effective thermal conductivity for each phase and $\nabla \langle T \rangle$ is the macroscopic temperature gradient. To compute this tensor, we performed a total of 3 simulations on the samples shown in Figures 4 and 5. A temperature difference was imposed on the walls along one of the three axes, while the other walls were kept adiabatic. The methodology is fully detailed in [8].

The boundary conditions are illustrated on the right in Figure 8 as an example of the heat flow in the Y direction. Using $\nabla \langle T \rangle$, we calculated $\boldsymbol{\phi}$. Water was used as the fluid phase, with a thermal conductivity of $\lambda_f = 0.62\,\mathrm{W\,m^{-1}\,K^{-1}}$, while the thermal properties of the PDMS polymer were considered for the solid phase, with $\lambda_s = 0.15\,\mathrm{W\,m^{-1}\,K^{-1}}$.

Eigenvalues of $\overline{\overline{\lambda_{\text{eff}}}}$ (Solide phase)	Eigenvalues of $\overline{\overline{\lambda_{\text{eff}}}}$ (Fluid phase)
0.038	0.548
0.038	0.566
0.042	0.579

Table 1 : *Eigenvalue decomposition of the solid and fluid tensor of the effective thermal conductivity.*

Table 1 shows the eigenvalues of the tensors for both solid and fluid phases. The solid phase deviates from isotropic character by less than 10%, while the fluid phase by than 6%. In the future, we plan to determine the effective thermal conductivity of the two phase system and explore the influence of different thermal conductivity ratios on the tensor associated to a single temperature model.

5. Permeability Tensor

To determine the permeability tensor, a mass flow rate was applied to one of the faces. The Reynolds number (Re), based on the Darcy velocity (U) and the pore diameter as characteristic size, was varied in the range of 0.005 to 105. The opposite face was set as a pressure outlet, while the remaining boundary conditions of the sample were modeled as slip walls, as seen in Fig. 8. These boundary conditions were repeated three times to perform numerical simulations with flow along the three directions. The components of the averaged pressure gradient and the average velocity gradient vector in each direction are used to determine the permeability tensors, as described in [8], through the following equation:

As shown in Figure 9, using the example of the z-direction flow, we can identify the Darcian flow regime by plotting the pressure loss as a function of the superficial velocity. A linear fit enables grouping the data points until deviations from the fit begin to affect the regression coefficient. From the first nine points (up to Re = 1.7) we are therefore able to identify the

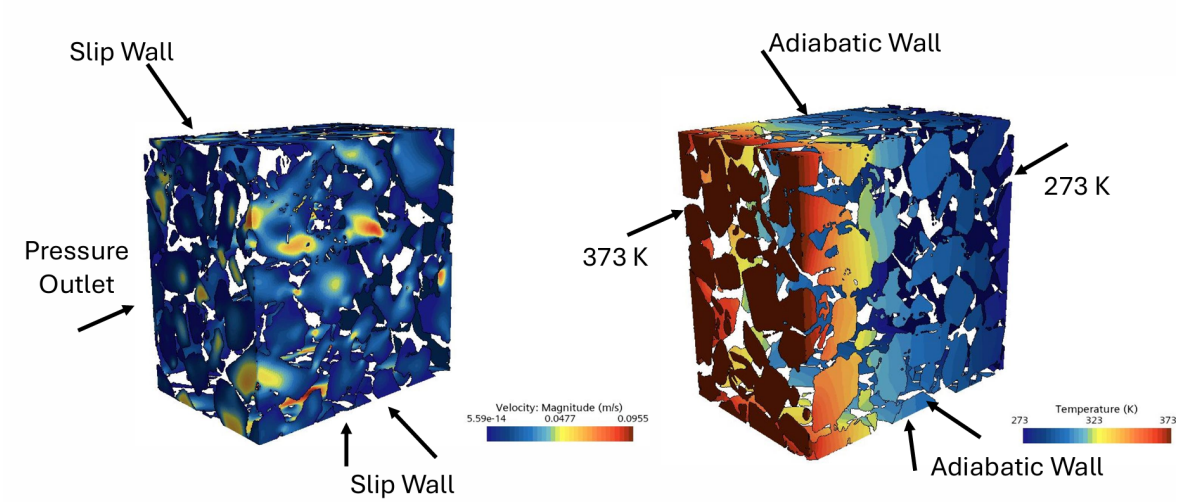

Figure 8 : *Example of the boundary conditions used to determine the mass flow (left) and thermal (right) properties of the PDMS porous medium. The left Figure shows the velocity field for Re = 5.02. On the right temperature distribution in y direction.*

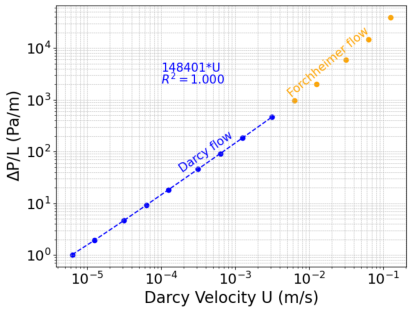

Figure 9 : *Pressure loss as a function of Darcy velocity, highlighting the range of the Darcy flow regime in the z direction.*

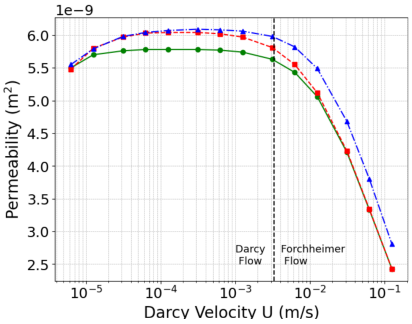

Figure 10 : *Apparent permeability tensor component versus Darcy velocity*

fitting coefficient (and thus K_D). Figure 10 shows the apparent permeability values for the three flow directions. A linear trend is visible for the first 9 points, corresponding to the Darcy flow regime. We do not try to identify the inertia coefficient due to the small Re range. The analysis of the deviation from the Darcy law will therefore be presented in future works.

6. Mass/Thermal Dispersion Tensor in the fluid phase

An important mechanism governing the mixing process in porous media is the accelerated diffusive mass transfer by the local enhancement of concentration gradients. Therefore, it is necessary to also investigate the hydrodynamic dispersion in such media, as it may dominate the mass transfer over diffusion, depending on the Péclet number (Pe). In the work of [10], a numerical simulation approach on the pore scale based on [9] was proposed. The main equation utilized for the calculation of the dispersion tensor $\mathbf{D}^*$ is based on the diffusivity coefficient D. Note that the following equations can be similarly applied to calculate thermal dispersion in the fluid phase:

$$\mathbf{D}^* = D\left(\mathbf{I} + \langle \nabla \mathbf{B} \rangle^f\right) - \langle \tilde{\mathbf{v}} \mathbf{B} \rangle^f. \tag{3}$$

Here the operator $\langle\rangle^f$ represents the volume average of a quantity over the occupied volume. The vector $\mathbf{B}$ is called closure variable, so that:

$$\tilde{\mathbf{v}} + \mathbf{v} \cdot \nabla \mathbf{B} = \nabla \cdot (D \nabla \mathbf{B}) \quad \text{in the computational domain,} \tag{4}$$

$$\mathbf{n} \cdot \nabla \mathbf{B} = -\mathbf{n} \quad \text{at the fluid/solid boundary.} \tag{5}$$

and $\tilde{\mathbf{v}}$ represents the deviation of the local velocity to the mean velocity. A detailed description of the utilized model can be found in [10].

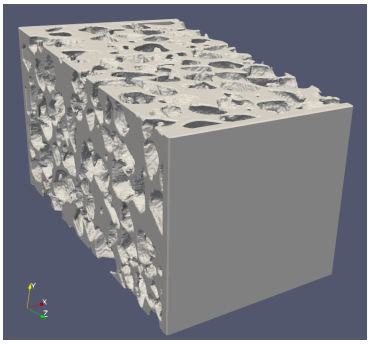

Figure 11 : *3D View of the numerical sample of sandstone used in both studies*

Since the geometry investigated in this work has not been previously analyzed in detail with respect to its mass transport properties, we selected two reference geometries with known dispersion values to validate the reliability of the chosen numerical tools. The proposed model is applicable only for periodic boundary conditions (solution of the homogenization problem). To ensure this, small buffer blocks are introduced at the inlet and outlet of the domain, as shown in Figure 11, to enforce periodicity. As the precise value of the characteristic length chosen for the Pe number was not known, we adjusted the Pe numbers from [10] to align with those calculated in our work. The equation for the fitting curve is provided in the legend of Figure 12. The deviation between the blue and orange points is less than 5%, which validates our tools for the set of equations considered. At low Péclet, molecular diffusion dominates dispersion for both geometries (Figure 12). The ratio $\frac{D^*}{D}$ remains constant and corresponds to the apparent molecular diffusion coefficient, which is lower than the true molecular diffusion coefficient due to the presence of the solid phase. For Pe>1 the effect of dispersion becomes visible. In the present case, the slope characterizing the PDMS porous medium is steeper than that of the sandstone, indicating a higher longitudinal dispersion rate at the same Péclet number. According to some authors [11], several factors influence dispersion, that depend on velocity, pore size distribution, shape and connectivity.

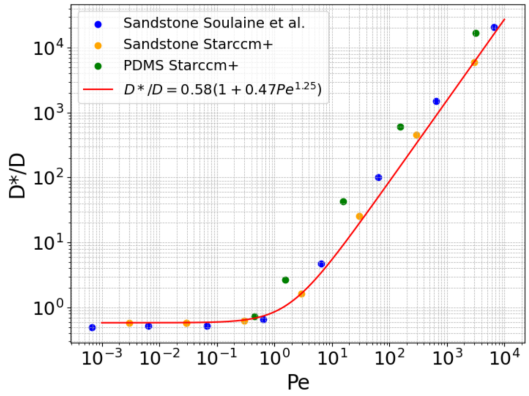

Figure 12 : *Comparison of the longitudinal component of the dispersion tensor for the sandpack, as calculated using StarCCM+, with the values reported in [10], and the corresponding preliminary values for the presented PDMS porous medium.*

7. Conclusion

The presented work outlines the method and workflow for the analysis of a novel polymer-based porous medium. The applied models and calculated properties shown are applicable to both mass and thermal transport studies. The primary objective is to analyze the entire domain based on the CT images described above and to investigate the potential dependencies between mass and heat dispersion, thermal conductivity, geometric properties (porosity, pore shape etc.) and the efficiency of the mixing process. Moreover, the influence of the size of the chosen ROI on these properties will be analyzed. The latter would indicate if the sample is an REV and could potentially give insights into the physical aspects of fluid mixing in porous media. In this context, it should be noted that the results for the PDMS sponge are preliminary at this stage.

References

[1] Chia-Yen Lee, Chin-Lung Chang, Yao-Nan Wang, Lung-Ming Fu, Microfluidic Mixing: A Review, *Int. J. Mol. Sci., 1422-0067, (2011) 3263-3287.*

[2] H. Bachman,C. Chen. J. Rufo,S. Zhao,S. Yang,Z. Tian, An acoustofluidic device for efficient mixing over a wide range of flow rates, *Lab Chip, 20, (2020) 1238-1248.*

[3] M. Bayareh, M. N. Ashani, A. Usefian, Active and passive micromixers: A comprehensive review, *Chem. Eng. Proc. - Proc. Inten., 147, (2020) 107771.*

[4] J.B. Kirby, Micro- and Nanoscale Fluid Mechanics: Transport in Microfluidic Devices, *Cambridge*, Cambridge University Press (2010).

[5] J. Heyman, D. R. Lester, R. Turuban, Y. Méheust, T. Le Borgne, Stretching and folding sustain microscale chemical gradients in porous media, *Proc. Nat. Acad. Sc., 117, (2020) 13359-13365.*

[6] E. Grigorov, B. Kirov, J. Denev, V. Galabov, Novel Approach for Passive Mixing in Microfluidics Utilizing Porous PDMS Sponge, *Int. Sc. Conf. Comp. Sc., 2, (Sozopol, June 2023) 1-6.*

[7] E. Brun, J. Vicente, F. Topin, R. Occelli, A 3D morphological tool to fully analyse all kind of cellular materials, *Cellmet08, 2, (Dresden, October 2008) 1-6.*

[8] Y. Jobic, P. Kumar. F. Topin, R. Occelli, Determining permeability tensors of porous media: A novel 'vector kinetic' numerical approach, *Int. J. Mult. Fl., 110, (2019) 198-217.*

[9] S. Whitaker, The Method of Volume Averaging, *Kluwer Academic Publisher, 13, (1999).*

[10] C. Soulaine, L. Girolami, L. Arbaret, S. Roman, Digital Rock Physics: computation of hydrodynamic dispersion, *Oil Gas Sci. Technol., 51, (2021) 198-217.*

[11] W.E. Brigham, P.W. Reed, J. N. Dew, Experiments on Mixing During Miscible Displacement in Porous Media., *SPE J. 1, 1, (1961) 1-8.*

Acknowledgements

We would like to thank **Cyprien Soulaine** for providing all the materials of his paper ([10]) and particularly the geometrical domain used, which enables us to validate our solution of the closure problem in complex porous domain. The authors acknowledge the ANR – FRANCE for its financial support of the TEGTIC project n°ANR23-CE51-0055.